Laser-Induced Fluorescence Measurement of the Ion-Energy-Distribution Function in a Collisionless Reconnection Experiment

A. Stark,[1] W. Fox,[2] J. Egedal,[2] O. Grulke,[1] and T. Klinger[1]

[1]*Max-Planck Institute for Plasma Physics, EURATOM Association, Greifswald 17491, Germany*

[2]*Massachusetts Institute of Technology, Plasma Science and Fusion Center, Cambridge 02139, Massachusetts, USA*

(Received 2 March 2005; revised manuscript received 2 August 2005; published 1 December 2005)

Observations in space and laboratory plasmas suggest magnetic reconnection as a mechanism for ion heating and formation of non-Maxwellian ion velocity distribution functions (IVDF). Laser-induced fluorescence measurements of the IVDF parallel to the X line of a periodically driven reconnection experiment are presented. A time-resolved analysis yields the evolution of the IVDF within a reconnection cycle. It is shown that reconnection causes a strong increase of the ion temperature, where the strongest increase is found at the maximum reconnection rate. Monte Carlo simulations demonstrate that ion heating is a consequence of the in-plane electric field that forms around the X line in response to reconnection.

DOI: 10.1103/PhysRevLett.95.235005 PACS numbers: 52.35.Vd, 52.72.+v

The rapid release of magnetic stress and magnetic energy through changes in the field line topology is known as reconnection [1]. Magnetic reconnection is likely to control the spatial and temporal evolution of explosive phenomena such as solar flares [2], coronal mass ejections [3], magnetic substorms in the geomagnetic tail [4], and internal disruptions in magnetic fusion devices [5]. Magnetic reconnection has been the subject of a vast number of theoretical investigations [6]. Already decades ago, magnetic reconnection was studied in the laboratory [7]. Dedicated experiments contributed much to a deeper understanding of the physics mechanisms [8,9]. However, the plasma dynamics and kinetics in the reconnection layer are still a conundrum; even the origin of the fast time scales under which collisionless magnetic reconnection is observed is not yet well understood [10]. Progress towards a better model description of the reconnection dynamics requires detailed observations of the plasma response with high temporal and spatial resolution. This is generally difficult to achieve in space and fusion plasmas, which motivates well-defined laboratory experiments with a tailored diagnostics instrumentation. Since simple MHD pictures tend to fail in the reconnection layer [11], the individual electron and ion kinetics during the reconnection process are of particular interest. The present Letter reports on the first laser-induced fluorescence (LIF) [12] measurements of the ion velocity distribution function (IVDF) in the reconnection layer.

The experiments were done in the Versatile Toroidal Facility (VTF) device [13], where the fast reconnection process is mediated by trapped electrons [14]. Recent *in situ* measurements obtained by the Wind spacecraft deep in the Earth's magnetotail are consistent with reconnection governed by similar trapped electron dynamics [15]. The collisionless argon plasma (electron density $n_e \simeq 1 \times 10^{17}$ m^{-3}, electron temperature $T_e \simeq 20$ eV, electron mean free path $\lambda_e \simeq 50$ m $\gg$ plasma dimensions) is created by electron cyclotron resonance heating (ECRH) at a frequency of 2.45 GHz and at typical output power of 20 kW. The vacuum magnetic field configuration of VTF forms an open cusp (with magnetic field lines intersecting the vessel walls) and reconnection is periodically driven at $f_d = 15$ kHz via an additional poloidal field coil [13], which makes the reconnection drive independent from plasma production. For the present study the poloidal magnetic field gradient (approximately constant across the device) is $|\nabla B_\theta| \simeq 50$ mT/m. A set of toroidal field coils creates the guide field $B_\phi \simeq 90$ mT. The induced toroidal electric field (equivalent to the reconnection rate) has a peak value of $E_\phi \simeq 10$ V/m, corresponding to a loop voltage of $U_{\mathrm{loop}} \simeq 65$ V. This reconnection drive provides in-plane flow in the plasma which approaches 10% of the in-plane Alfvén speed; the relevant Alfvén speed is evaluated with the in-plane magnetic field at the edge of the diffusion region (2 cm from the X line).

The intrinsically high spatial resolution of LIF allows one to perform local measurements of the IVDF. The laser is aligned to measure in the diffusion region around the X line the ion velocity component $v_\parallel$ parallel to the toroidal guiding magnetic field B_ϕ. The size of the observation volume ($r \approx 1$ mm) is much smaller than the size of the diffusion region ($\delta \sim 4$ cm). The metastable argon II ion transition $3d^4F_{7/2} \rightarrow 4p^4D^0_{5/2}$ at $\lambda = 668.614$ nm is pumped by a diode laser (60 mW cw, 1 MHz bandwidth). Via photomultiplier tube (PMT) and interference filter (1 nm bandwidth), the fluorescence signal of the transition $4p^4D^0_{5/2} \rightarrow 4s^4P_{3/2}$ at $\lambda = 442.72$ nm is recorded.

Figure 1 summarizes the LIF measurement procedure for obtaining time-resolved IVDFs. The laser light is chopped "on/off" at a frequency $f_d/2 = 7.5$ kHz and phase locked to the reconnection drive, which means that two reconnection periods are driven during each laser on-off cycle (see Fig. 1). The LIF signal is obtained by

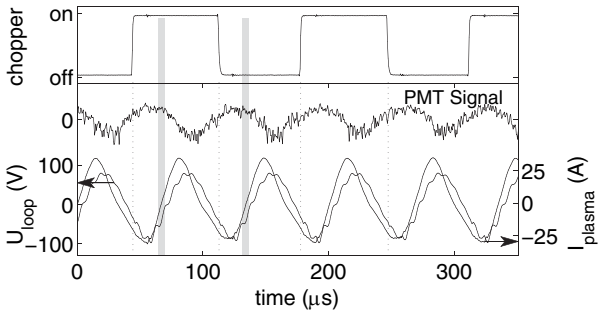

FIG. 1. Chopper signal (top trace), PMT signal fluctuations (middle trace), and loop voltage U_{loop} and total plasma current I_{plasma} (bottom traces).

discriminating between the signals recorded with the laser on and laser off, respectively. For each laser wavelength λ, data from typically 30 reproducible plasma discharges are combined to obtain adequate signal to noise ratio. Tuning the laser over a suitable wavelength range yields the complete IVDF. Synchronizing chopper and drive allows for phase-locked averaging and thereby to resolve the fast time scale of the reconnection cycle (the time resolution of $\Delta t = 5$ μs is restricted by the signal to noise ratio).

The amplitude evolution of the periodically induced toroidal plasma current during a VTF shot, shown in Fig. 2(a), is obtained by Hilbert transform of $I_{\text{plasma}}(t)$. Figure 2(b) depicts the root mean square (rms) PMT fluctuation signal. For comparison, the rms PMT signal without the reconnection drive is included in the figure (gray curve). The voltage on the capacitor bank powering the reconnection drive decreases about 50% during the discharge. The reconnection drive amplitude is therefore decreasing too, which leads to a decrease of the rms values of the PMT fluctuation signal. At large reconnection drive amplitudes, in the time interval 10–40 ms, it is observed that reconnection causes a significant increase of the light emission fluctuations at 442 nm, far above the base level.

Figure 3 shows the measurement of the IVDF with and without reconnection drive (square and diamond markers, respectively), averaged over ten identical discharges. The least-square fit of a Gaussian (including Zeeman splitting) to the data points and the respective residua are also shown in the diagram. If reconnection is driven, there is an increase of the ion temperature from $T_i = 0.5$ eV to 1.1 eV ($\pm$ 7% uncertainty). Ion heating caused by reconnection was recently observed in the MRX device [16] and in the spheromak devices SSX [17] and TS-3 [18]. Ion energy balance calculations suggested that ion heating is caused by viscous heating and by nonclassical dissipation processes. In addition to the ion temperature increase, the mean drift velocity raises in VTF from $v_d = 0.29 c_s$ to $v_d = 0.44 c_s$, where $c_s = \sqrt{T_e/m_i}$ is the ion sound speed. Toroidal ion drifts of the same order of magnitude were observed by Mach probes.

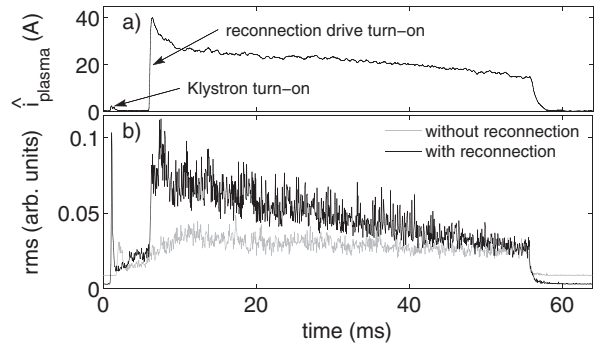

FIG. 2. A typical VTF shot with approximately 750 reconnection cycles. (a) Time evolution of the toroidal plasma current amplitude $\hat{i}_{\text{plasma}}(t)$. (b) PMT fluctuation signal rms value with and without the reconnection drive (black and gray line, respectively).

To establish a causality between the reconnection rate and the increase of the ion temperature, either amplitude or frequency of the reconnection drive must be varied. While the frequency is fixed by design parameters of the resonance circuit, the amplitude inherently varies by 50% during a VTF shot [cf. Fig. 2(a)]. It is thus reasonable to measure the IVDF time resolved over a discharge. To improve statistics, the average over 30 identical discharges is taken.

The measured data is divided into consecutive intervals of $\Delta t = 5$ ms length. The resulting time evolution of the IVDF is shown in Fig. 4; its thermal component yields the ion temperature evolution [Fig. 4(a)]. In the case without reconnection a constant ion temperature of $T_i \simeq 0.3$ eV is found within the entire shot. A different situation emerges if reconnection is driven: From $t = 5 \ldots 15$ ms the ion temperature rapidly rises from $T_i \simeq 1$ to 2 eV, and gradually drops to $T_i \simeq 1$ eV at $t = 60$ ms. This development correlates well with the temporal behavior of the reconnection drive amplitude [Fig. 2(a)].

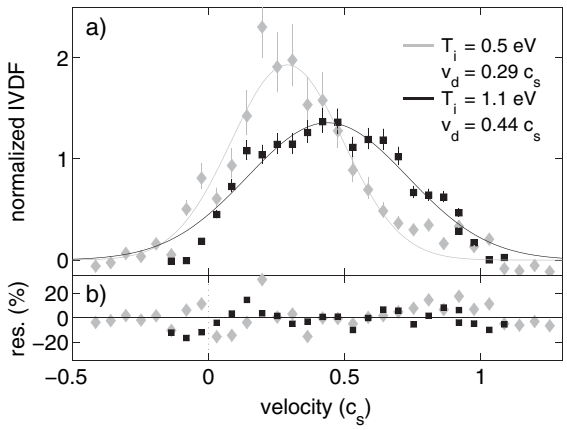

FIG. 3. (a) LIF measurements of the IVDF and the ion temperature. Error bars are obtained from the 95% confidence interval of the periodogram estimation. Gaussians are fitted to the measured data: without reconnection (gray diamonds) and with reconnection (black squares). (b) Residua (in %) show the goodness of the two least-square fits.

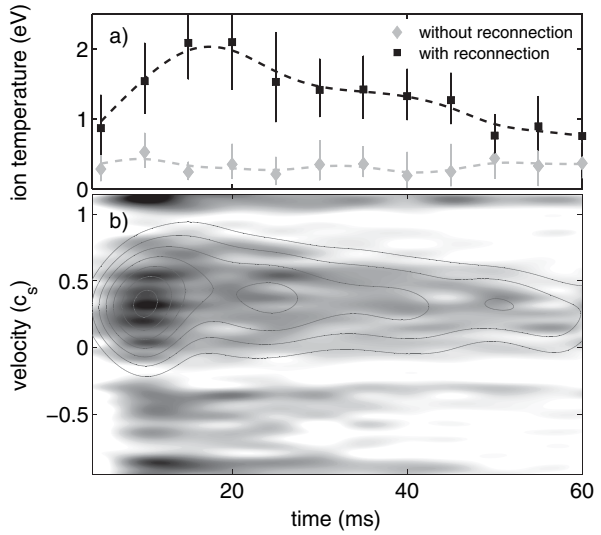

FIG. 4. (a) Time evolution of the ion temperature T_i during a VTF shot (cf. Fig. 2): without reconnection (gray diamonds) and with reconnection (black squares). Spline fits (dashed lines) are included to guide the eye. (b) Gray scale plot of the time evolution of the IVDF during a VTF shot. Contours of Gaussians fitted to the thermal component are indicated as solid lines.

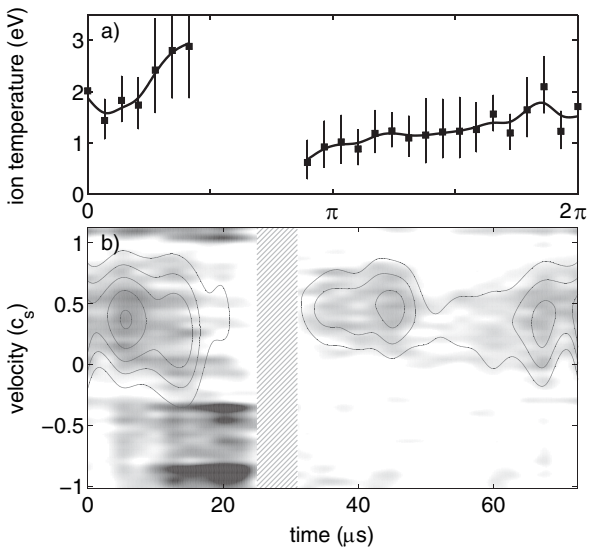

FIG. 5. (a) Phase resolved measurement of the ion temperature T_i (black squares with spline fits). (b) Evolution of the IVDF during a reconnection cycle: Shown are the raw data (gray shaded plot) and contours of thermal component fitted by Gaussians (solid lines). The hatched area indicates the interval where no LIF signal is obtained.

Without reconnection drive one observes a thermal IVDF only. In contrast, driven reconnection leads to strong nonthermal components in the tail regions of the IVDF. This is shown in Fig. 4(b) where the scan range of the laser was enlarged to its technical limits in order to explore the tail regions of the IVDF. The IVDF is plotted in gray scale; contour lines indicate the Gaussians fitted to the thermal component. The amplitude development of both the thermal and the beam components is a consequence of the decreasing plasma density, owing to decreasing ECRH output power. Beam components are found to be symmetrically located at $\pm 0.7 c_s$ and at $-1.3 c_s$ relative to the center of the IVDF's thermal component. It is reasonable to expect also a beam at $+1.3 c_s$, which is out of the laser tuning range. It turns out that the number density of the beams is almost equal to the number density of the thermal component.

So far it has been demonstrated that reconnection is linked to both an increase of the ion temperature and the occurrence of strong nonthermal components. But it remains unclear whether both effects are interlinked. To address that question we investigate the evolution of the IVDF during a single period of the reconnection drive. That analysis is restricted to the time interval $t = 10 \ldots 30$ ms where reconnection strongly affects the ion dynamics [cf. Fig. 4(a)]. Figure 5(a) shows the evolution of the ion temperature during one reconnection cycle (black squares). The ion temperature varies significantly from $T_i = 0.5$ eV at phase $\phi \simeq \pi$ to $T_i = 3$ eV at $\phi \simeq \pi/2$. In between, the ion temperature rises monotonously. The data gap $\phi \simeq \pi/2 \ldots \pi$ is due to the depletion of the thermal component as seen in Fig. 5(b). Included in that plot is the raw data of the IVDF (gray shaded) and contours of the Gaussians fitted to the thermal component (solid lines). The hatched area marks the phase interval, where the LIF intensity drops due to the (eclipselike) on-off transition of the chopped laser light. The beam components are observed just in a small interval around the minimum loop voltage at $t \simeq 15$ μs. Their velocity spread is fairly small. The number density of the beams is twice as high as the bulk number density. Correlated with the sudden appearance of the beams is a rapid increase of the ion temperature from $T_i \simeq 2$ to 3 eV and a depletion of the bulk number density. At $t \simeq 35$ μs the bulk density recovers but at a much lower ion temperature. Within the reconnection cycle there is an asymmetry; i.e., in the phase interval $[\pi, 2\pi]$ no beam components are observed and the depletion of the bulk number density is much less developed.

The reconnection electric field E_ϕ ($\approx$10 V/m) is far too small to generate the observed heating; thermal particles can gain only about 0.1 eV between collisions due to this field. However, the in-plane electric field which forms in response to the reconnection (to maintain $\mathbf{E} \cdot \mathbf{B} = 0$ away from the X line [14,19]) is much larger, nearly 1 kV/m (see top part of Fig. 6).

To investigate the ion heating during reconnection, we have written a test-particle simulation which numerically integrates particle orbits in the in-plane fields, using the potential $\Phi = E_\phi l_0/4 \times \log((x^2 + \delta^2)/(y^2 + \delta^2))$, see [19] Eq. (1). The fields are not only large, but vary rapidly in space near the X point. Numerically we have found that the dimensionless parameter $e\nabla^2\Phi\rho_i^2/m v_{ti}^2$ ($\sim$3 for these experiments) controls the heating. When this parameter is

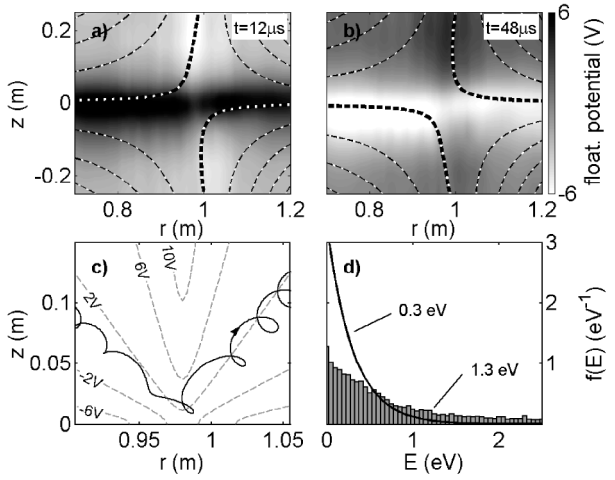

FIG. 6. Probe measurements of the perpendicular electric potential at two separate time instants, $t = 12$ (a) and $t = 48$ μs (b). Pairs of magnetic field lines (dashed lines) are plotted bold to indicate the poloidal motion of the magnetic flux. (c) Calculated orbit of a ion (going left to right) in the in-plane fields at the X line. (d) Histogram of the energy distribution of ions with initial energy $f(\mathcal{E}) = 0.3$ eV (solid line) after passing the X line once.

larger than unity the magnetic moment of the ions is not conserved, leading to perpendicular heating.

Figure 6(c) shows a typical orbit. The particle, starting with perpendicular energy $\mathcal{E} = 0.3$ eV, leaves the reconnection region with $\mathcal{E} \approx 1.15$ eV. Orbits through the reconnection region depend sensitively on the initial location and initial gyrophase, hallmarks of the nonlinear dynamics of the system. Figure 6(d) shows the energy distribution $f(\mathcal{E})$ (the histogram) after one pass through the X line, given an initial thermal distribution at 0.3 eV and averaged over the initial gyrophase and position. The final distribution has a tail compared to a thermal distribution: the average energy $\langle\mathcal{E}\rangle = \int \mathcal{E} f(\mathcal{E}) d\mathcal{E}$ is 1.3 eV. Three passes are sufficient to heat the particles from 0.3 to 2 eV. Consistent with the electrostatic probe measurements, for these simulations, we have used the parameters $eE_\phi l_0 = 8$ eV, and $\delta = 0.84$ cm.

The in-plane electric fields are capable of heating the plasma in the perpendicular direction, but in LIF measurements it is observed heating parallel to the magnetic field. However, the ion-ion collision frequency ν_{ii} evaluated for singly-charged argon ions at $n = 5 \times 10^{16}$ m^{-3} ranges from 30×10^3 s^{-1}($\approx f_{ci}$) at 0.3 eV to 2×10^3 s^{-1} at 2 eV. Since the heating of the ions occurs within 1–2 gyroperiods near the X line, the perpendicular fields are able to heat, while the collisions transfer perpendicular to parallel heating. In fact, classical viscous heating is dominating at low energies, but it is the collisionless heating mechanism that controls the total final temperature.

Finally, the oscillating reconnection drive is a substantial fraction of the ion cyclotron frequency ($f_d = 0.45 f_{ci}$). This pushes particles multiple times through the X point, allowing for multiple passes of heating. However, it is the sharp spatial variation of Φ that breaks the adiabatic invariant μ, not its oscillation in time. In the present scenario, a toroidal volume with a cross section diameter of about 5 cm is driven back and forth across the X-line region. Assuming that each ion in this volume is energized on average 1 eV per transition, about 3 W of the dissipated energy goes to ion heating. In comparison, the total dissipation in the reconnection region is $\langle I_{\text{plasma}} U_{\text{loop}} \rangle \sim 1.3$ kW (channeled to the electrons carrying the plasma current). In turn, this number is small compared to the integral of the Poynting flux $\int (\mathbf{E} \times \mathbf{B}/\mu_0) dS \sim 1$ MW passing across the separatrix (within 10 cm from the X line).

To summarize, the ion velocity distribution function was measured with LIF in a reconnection experiment. Ion heating on the timescale of the reconnection drive was observed and is found to scale with the amplitude of the reconnection drive. In addition, nonthermal beam components were observed. Particle simulations reveal that ions passing the X-line region in the perpendicular direction are effectively heated by the in-plane electric field. Ion-ion collisions then lead to the observed parallel heating by a factor of 3–5, localized at the X line only. The in-plane electric fields are a general feature of reconnection with a strong guide magnetic field, emphasizing the importance of the present observations.

[1] J. W. Dungey, Philos. Mag. **44**, 725 (1953).
[2] S. Masuda *et al.*, Nature (London) **371**, 495 (1994).
[3] T. D. Phan *et al.*, Nature (London) **404**, 848 (2000).
[4] V. M. Vasyliunas, Rev. Geophys. Space Phys. **13**, 303 (1975).
[5] J. B. Taylor, Rev. Mod. Phys. **58**, 741 (1986).
[6] D. Biskamp, *Magnetic Reconnection in Plasmas* (Cambridge University Press, Cambridge, England, 2000).
[7] R. L. Stenzel and W. Gekelman, Phys. Rev. Lett. **42**, 1055 (1979).
[8] Y. Ono *et al.*, Phys. Rev. Lett. **76**, 3328 (1996); Y. Ono *et al.*, Phys. Plasmas **4**, 1953 (1997).
[9] M. Yamada *et al.*, Phys. Rev. Lett. **78**, 3117 (1997); M. Yamada *et al.*, Phys. Plasmas **4**, 1936 (1997).
[10] P. A. Sweet, Nuovo Cimento Suppl. **8**, 188 (1958); E. N. Parker, J. Geophys. Res. **62**, 509 (1957); R. M. Kulsrud, Phys. Plasmas **2**, 1735 (1995).
[11] M. Yamada *et al.*, Phys. Plasmas **7**, 1781 (2000).
[12] R. Stern and J. Johnson, Phys. Rev. Lett. **34**, 1548 (1975).
[13] J. Egedal *et al.*, Rev. Sci. Instrum. **71**, 3351 (2000).
[14] J. Egedal *et al.*, Phys. Plasmas **11**, 2844 (2004).
[15] J. Egedal *et al.*, Phys. Rev. Lett. **94**, 025006 (2005).
[16] S. C. Hsu *et al.*, Phys. Rev. Lett. **84**, 3859 (2000).
[17] M. R. Brown *et al.*, Phys. Plasmas **9**, 2077 (2002).
[18] Y. Ono *et al.*, Phys. Rev. Lett. **76**, 3328 (1996).
[19] J. Egedal *et al.*, Phys. Rev. Lett. **90**, 135003 (2003).